International Journal of Computational Vision and Biomechanics
Vol. 5 No. 1 (January-June, 2019)

MUK PUBLICATIONS
Open Access Publisher

A Framework for 3D Reconstruction of Human Organs from MR Images: A Model and Fuzzy Set Principles Based Approach. Application to Prostate Segmentation and Reconstruction

Betrouni N.[1] & Vermandel M.[1]

[1]*Inserm, U703, Medical Technology Institute, CHRU Lille, France.*

Faculty of Medicine, University of Lille II, UPRES EA 1049, Lille, France.

Submitted: 16th December 2018 *Revised: 25th January 2019* *Accepted: 06th April 2019*

In this work we present a method for automatic 3D segmentation of prostate on MR images and volume reconstruction by fuzzy sets fusion algorithm. The segmentation is model based method and the reconstruction takes into account the slice thickness to reduce the partial volume effect. The tool is applied for prostate segmentation in radiotherapy planning.

Keywords : 3D segmentation, deformable model, Fuzzy sets reconstruction, Prostate, MRI

I. INTRODUCTION

3D segmentation and reconstruction is a difficult process because they must take into account the different deformations which characterize the object to be segmented. In the medical field, manual body delineation is a time consuming task and often requires prior knowledge to cope absence of contours due to the lack of contrast of images as well as the great variability of body shapes and positions. For these reasons, researches in this field were directed towards methods which combine image information and *a priori* knowledge about the structure of the studied object. These methods are an extension of active contours ([1], [2]) and can be classified in two classes:

Methods with a priori knowledge on the geometry: The first work was that of [3] and its 3D extension in [4], [5] and [6] and m-reps multiscale description introduced by [7].

Methods with a priori knowledge on appearance: In this category, in addition of information about the geometry of the object, information on its appearance, in particular gray levels and textures are included [8] and [9] where knowledge about the probabilities densities of the pixels inside the form is added.

In many medical fields, the needs for segmentation are very important. In this paper, we propose a general framework for 3D reconstruction of human organs from MRI. This framework is described here through the process of prostate segmentation and reconstruction for prostate cancer diagnosis and image-guided therapy planning. Because automatic prostate segmentation remains complicated-in particular at apex either from transrectal ultrasound images (used for brachytherapy) or from MRI or CT (used for radiotherapy)-it seems to be an appropriate field of application of our approach.

This article is presented as follow: first, we shortly present the context of prostate segmentation for radiotherapy planning, then we detail the model-based approach and the fuzzy set principles method used for reconstruction.

II. CONTEXT

For image guided therapy, some solutions appeared and especially to be applied in clinical practice. In [10], the authors proposed a method to segment the bladder, the rectum and the femoral heads on CT images. The method is based on a 3D model and user interaction to correct erroneous contour. Deformable image registration is a technique used in prostate segmentation in ([11], [12], [13], [14], [9]).

Considering the emerging role of MR imaging in radiotherapy treatment planning and the non-existence of a complete solution to assist the physician in target delineation i.e. prostate, we have designed an automatic segmentation tools based on a two steps framework. First, the prostate is automatically delineated using a deformable model algorithm. An implementation of the delineation algorithm was evaluated by comparing the results to manual segmentations made by a senor radiologist on images of 24 patients. Then, after the prostate is delineated, in order to perform a more realistic reconstruction and quantification of the prostate, we use a fuzzy set based algorithm [15]. This second step takes into account the partial volume effect and the MRI signal properties in a slice in order to obtain a volume closer to the physical one.

III. METHODS

3.1 Prostate Delineation with a Deformable Model

In a precedent report we have described a model based automatic prostate segmentation from ultrasound images combining an adaptive morphological filtering and a heuristic optimisation algorithm ([16]). We propose here an adaptation of this algorithm for 3D model-based

segmentation of prostate on MR images. Prostate model was trained based on manual segmentations from N = 15 patients MRI images that did not include the targets. According to the slice thickness and to its size and its shape, the prostate often appears on 8 to 12 slices in standard pelvic MR exam. In order to get a 3D model, the prostate was contoured, on each slice, by placing 20 points represented by their 3D coordinates $p_i = (x_i, y_i, z_i)$. Thus, the prostate surface was modellised by a vector $X = [x_0, y_0, z_0, x_1, y_1, z_1 \ldots, x_P, y_P, z_P]$, where P is the total number of surface points. For this study, whatever the number of slices used the total number of prostate points P was brought to 200.

Twenty points were used to describe each 2D contour as a compromise between the time spending and a detailed description of the contour variation. It should be underlined that this number of points is higher than the number of points usually laid out by the experts for delineating the prostate for radiotherapy purposes.

As the training set contained intra-patients data and the modelisation process was based on the variation of the positions of points over the set, it was important to align the points in the same way according to a set of axes. This alignment (rotation, translation and scaling) was achieved using the Iterative Closest Point (ICP) algorithm [17]. The ICP is based on an iterative alignment of the points through the minimization of a cost function which is the quadratic distance between the points. The method alternates pairing and calculation of the transformation between the paired points. Pairing is done by associating each point to its nearest neighbour.

(a) Extraction of statistical information

Principal Component Analysis (PCA) enabled us to extract the model shape and the most important modes [3] of deformation. Model shape of the N-contours was computed as the mean $\overline{X}$ of the vectors components:

$$\overline{X} = \frac{1}{N}\sum_{i=1}^{N} X_i \tag{1}$$

Main variations around mean shape correspond to eigen values of the covariance matrix S:

$$S = \frac{1}{N-1}\sum_{i=1}^{i=N} dX_i \overline{dX_i} \tag{2}$$

wherein

$$dX_i = X_i - \overline{X} \tag{3}$$

is the displacement vector.

Each eigenvector is responsible for a variance equal to its eigen value. Its contribution to total shape variation can be expressed as:

$$\alpha_k = \frac{\lambda_k}{\sum_{i=1}^{3P}\lambda_i} \tag{4}$$

wherein λ_k and α_k represent eigen values and eigenvectors contribution to shape variance respectively. The method of determining the main modes of deformation consists in decomposing the displacement vector on an orthonormal base:

$$dX = \sum_{i=1}^{3P} b_i \theta_i \tag{5}$$

wherein $\{\theta_i\}$ i = 1.. $3P$ are the base vectors and b_i represented the coordinates of vector dX in this base.

This decomposition was carried out using the Karhunen–Loeve transform [18], which consists in decomposing a random vector according to the eigenvectors of its covariance matrix:

$$S\phi_i = \lambda_i \phi_i \tag{6}$$

wherein λ_i represents the normalized eigen values of the covariance matrix S and ϕ_i its eigenvectors. These eigen values represent the variances of parameters b_i. An approximation of displacement vector dX was obtained through linear combination of m eigenvectors of covariance matrix S. These eigenvectors corresponded to the m most representative eigen values λ_i such as:

$$\sum_{i=1}^{i=m} \alpha_i \cong 1 \tag{7}$$

Thus a displacement vector can be expressed as:

$$dX \cong \sum_{i=1}^{m} b_i \phi_i \tag{8}$$

b- Model

Let $\phi = (\phi_1, \phi_2, \ldots, \phi_m)$ the matrix composed by m most important eigenvectors of S, a vector X can be expressed as:

$$X = \overline{X} + \phi b \tag{9}$$

wherein $b = \{b_i\}$ is a R^m vector.

Assuming that the distribution of the ϕ_i components is gaussian, all vector b component is included in $\pm a\sqrt{\lambda_i}$ interval. Interval limits were used for restraining model deformation. Then, organ segmentation consists in finding the m deformation parameters b_i and the interval parameter a, that characterize its contour.

Figure 1 shows the 3D rendering of the prostate model.

c- Contour searching

Contour searching was realised by optimising an energy function.

Contour energy

An energy defined by Terzopoulos *et al.* [2] is associated with each contour C:

$$E(C) = E_{\text{internal}} - E_{\text{external}} \tag{10}$$

The internal energy E_{internal} represents length and elasticity of the contour. The external energy E_{external} is

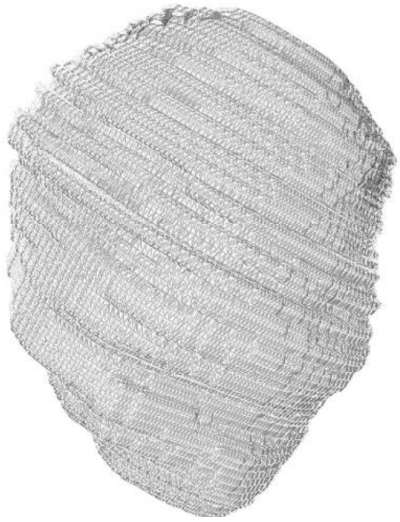

Figure 1: Prostate Model Rendering

associated with the image data. Its minimization tends the contour to recover the lines of steepest gradient. It's expressed as:

$$E_{external} = \int_a^b |\nabla|(v(s))|^2 \, ds \qquad (11)$$

wherein ∇I represents the image gradient calculated using the Deriche operator [19].

Contour optimization

Segmentation began with interactive initialisation to position the model over the target in the image using axial and sagittal sequences. The second stage consisted in iteratively searching for the final contour. This search was performed by a simulated annealing algorithm known for its ability to explore a large range of parameters [20]. At each step, a new parameters b_i vector was randomly generated and introduced in Eq. (9) to form a new contour and compute its energy. If the visually assessed delineation accuracy was insufficient, the procedure was repeated until a visual match between the deformable prostate model and the organ was reached. These interactive corrections were only used in the areas of large mismatch, where the model was attracted to close structures.

Figure 2 shows an example of prostate automatic delineation.

3.2 Evaluation of Automatic Delineation

The delineation method was evaluated by comparing the results to manual segmentations performed by a senor physician involved in the management of prostate cancer. He operated on an images base of 24 patients with prostate cancer. Images were acquired on a 1.5 T Philips Intera® scanner with a phased array coil, with the following sequence parameters: a sagittal T2-w Turbo Spin Echo (TSE) (Field of view (FOV) = 24 cm x 24 cm, matrix 512 x 512, Time Repetition (TR)/Time Echo (TE) = 1630/110 ms, Echo Train Length (ETL) = 16, Slice Thickness (ST) = 4 mm) and a T1-w 3D Fast Field Echo (FFE) (FOV = 40 cm x 40 cm, matrix 512 x 512, TR/TE = 25/4.5 ms, ST = 5 mm) or a T1-w TSE SENSE (FOV = 40 cm x 40 cm, matrix 512 x 512, TR/TE = 499/12 ms, ETL = 5, ST = 5 mm).

The comparison between manual and automatic delineation was made on ARTIView™ software

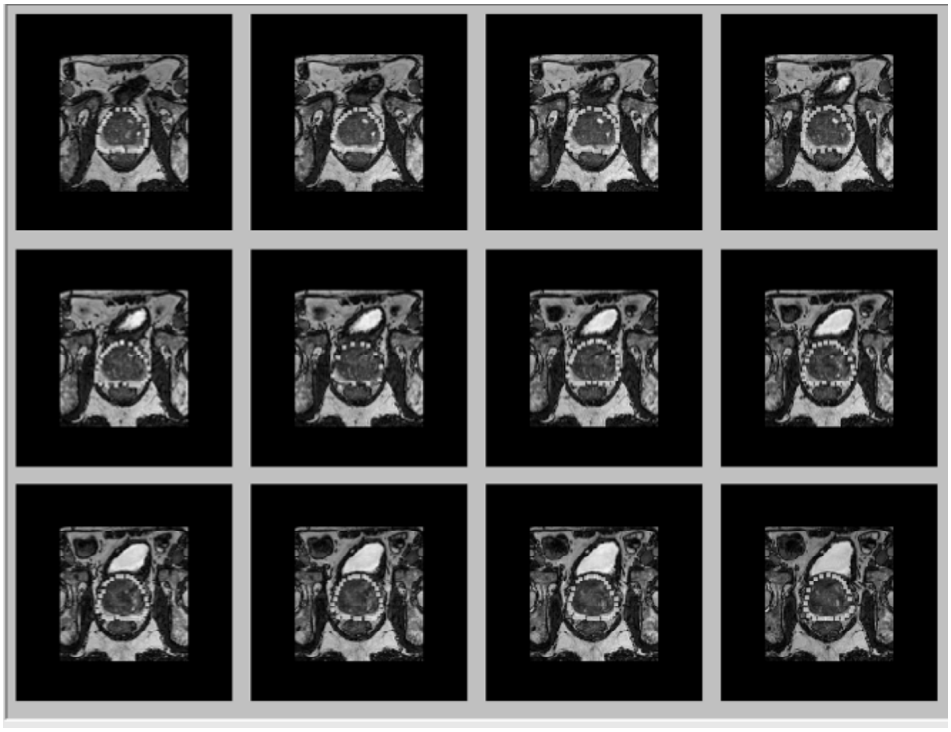

Figure 2: Example of Automatic Prostate Delineation on MR Images

(AQUILAB®SAS). This program identified the pixels located inside or outside a contour and assigned them a 0 or 1 value, respectively. The method was iterated for each slice of a given set of MR images. The following parameters were measured:

Volumes Ratio (Automatic/Manual)

Volume Overlap (ratio of the volume of intersection to the volume of union, optimal value = 1)

$$VO = \frac{Vm \cap Va}{Vm \cup Va} \tag{12}$$

VO = volume overlap, Vm = manual volume, Va = automatic volume

It's important to stress that this index is very sensitive to small variations in overlap because it is normalized to the union of the volumes. As an example, if two equal volumes overlap by 85% of each, the volume overlap would be only 0.74.

Correctly delineated volume (percent ratio of the volume of intersection to the manual defined volume, optimal value = 100);

$$VC = \frac{Vm \cap Va}{Vm} \tag{13}$$

VC = correctly delineated volume.

3.3 Prostate 3D reconstruction

Once the volume was delineated, we performed a 3D reconstruction which takes into account the slice profile and the 3-D neighboring [15]. This algorithm, using fuzzy set tools, enabled to perform a more realistic reconstruction. This algorithm was previously validated for radiotherapy planning [15] and for cerebral vessels segmentation on MR images [21].

The aim was to define, for each slice, a minimum region within which was surely inside the structure (i.e. prostate in this application), and a maximum region which was surely outside this structure. A degree of membership equal to one (1) was, thus, assigned to the pixels inside the minimum volume, and a degree of membership equal to zero (0) was assigned to the pixels outside the maximum volume (figure 3). The degree of membership of the pixels in the intermediate area was obtained with the theory of possibility [22] using distribution functions taking into account:

(1) the gray levels and the orientation of their local gradient in the image
(2) the local CNR in the vicinity of the intermediate area

The degree of membership of a given pixel within the fuzzy area was determined in considering the distribution of the gray levels between the external and the internal border (figure 4). Thus, for a given pixel among the distribution, the gray level is converted to a degree of membership according to a distribution (triangular, trapezoidal, exponential, etc.) As proposed in [15], we used a sigmoid distribution given by:

$$\mu = \begin{cases} 1 & \text{if } Gl \geq Max \\ 1 - \dfrac{(Gl - Max)^2}{2 \cdot \alpha^2} & \text{if } Max \geq Gl \geq c \\ \dfrac{(Gl - Min)^2}{2 \cdot \alpha^2} & \text{if } c \geq Gl \geq Min \\ 0 & \text{if } Gl \leq Min \end{cases} \tag{14}$$

where: $c = \dfrac{\text{Min} + \text{Max}}{2}$ and $|\alpha| = |c - \text{Min}| = |c - \text{Max}|$,

Gl is the gray level of a given pixel, Max and Min are the minimum and the maximum gray level among the distribution as shown figure. 6

Eq. 14 assigned to each pixel of each slice a degree of membership. In the case of a heterogeneous contrast around the structure, the pixel degree of membership of this structure should be greater in the higher-contrast area than in the lower-contrast area. Therefore, the membership distribution function has to be weighted as a function of contrast (Eq. 15). To do so, the CNR was calculated locally for each of the pixels belonging to the fuzziness region. This was achieved by calculating the local contrast along the structure boundary, taking a measurement of the noise in a local area, in the neighbourhood of the volume. The weighting function was then given by Eq. 15.

$$W_S = 1 - exp(-\alpha \, x \, CNR_S) \tag{15}$$
$$\mu' = W_S \, x \, \mu$$

where Ws is the weighting factor according to the CNR in the area (α is fixed at Log(100)/CNRMax so that WS = 0.99 for the higher CNRMax value observed in the whole set of MRA images) and μ' is the weighted degree of membership.

To take into account the slice thickness and the volume partial effect, all the pixels from all the slices were considered

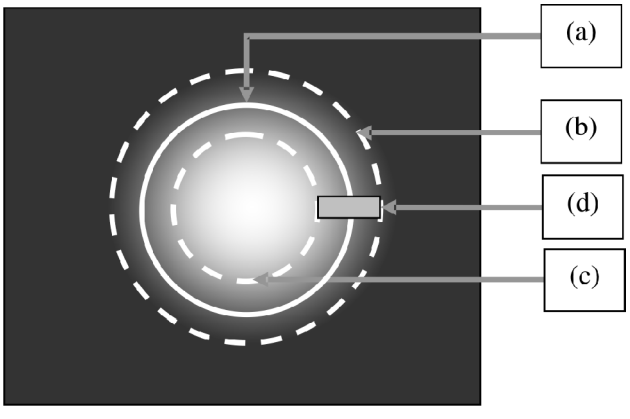

Figure 3: Definition of Fuzzy area Derived from the Initial Contour. (a) Initial Contour, (b) External Border of the Vascular Structure Obtained in Dilating (a) and Outside of which the Membership being Equal to 0. (c) Internal Border Obtained in Eroding (a) and Inside of which the degree of Membership being equal to 1. (d) Fuzzy Area.

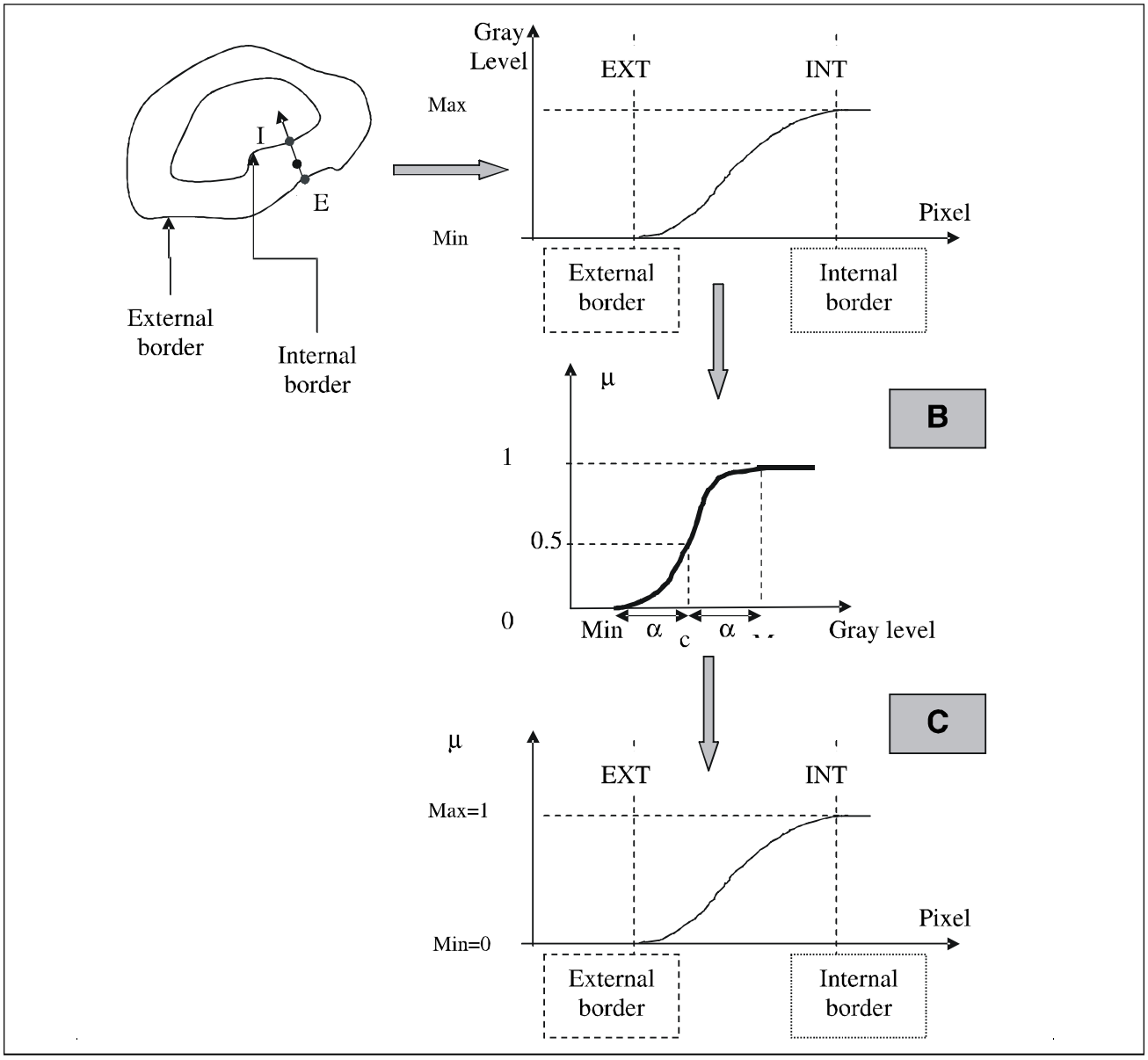

Figure 4: Computation of the Degree of Membership of the Pixels within the Fuzzy Area. For a given point of the External Border, the Gray Level Distribution is Measured (A) and is used to Convert the Pixels Gray Level into Degree of Membership (C). The Conversion from Gray Level to Degree of Membership is Achieved using a Sigmoid Function (B) (see Eq. 14). Note that in this Example, the Sigmoid Function is given for Dark Background and Bright Structure.

as voxels having a degree of membership to the structure. The first step in this 3-D process was the over-sampling of the volume according to the slice thickness (figure 5) and to take into account the slice profile of signal sensitivity (figure 6). This MR slice sensitivity profile was previously obtained by measurements taken on a phantom of known geometry [16].

Once this over-sampling performed, the degree of membership of each voxel μ',obtained from Eq. 15, was attributed to all the sub-voxels, weighted by signal sensitivity distribution into the slice as well as by the simultaneous contribution of the neighbouring slices (figure 6). For the sub-voxel n belonging to the slice i, we finally obtained the degree of membership μ_n":

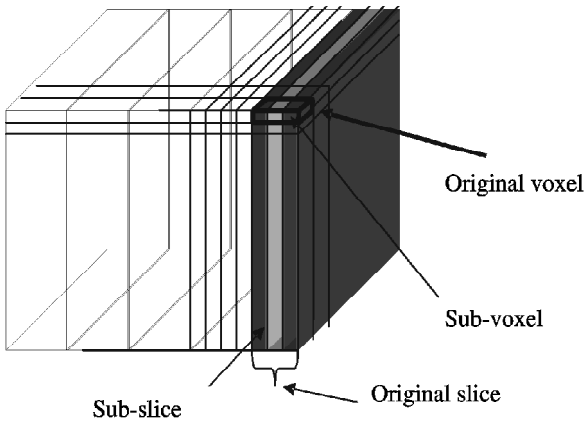

Figure 5: Over-sampling the Volume to Obtain Sub-voxels.

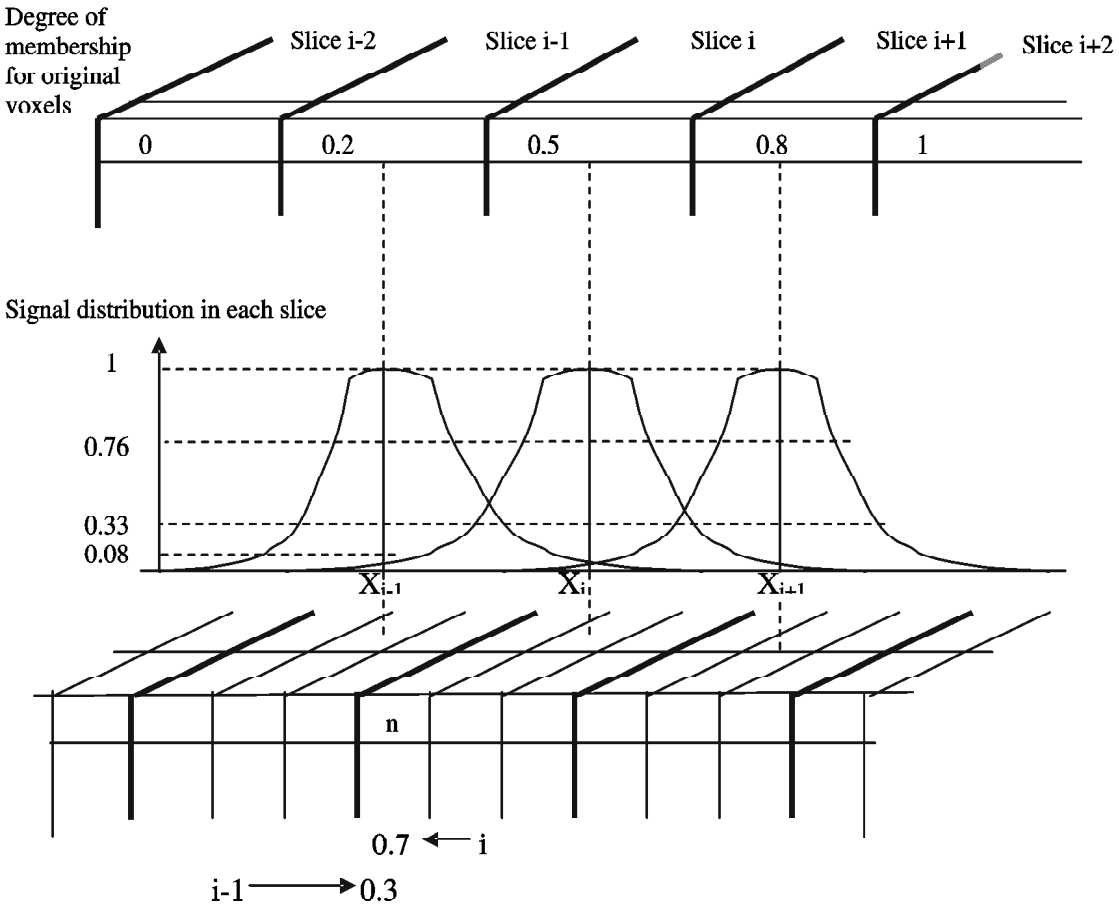

Figure 6: Signal distribution in the slices and contribution of contiguous slices to the calculation of membership for the sub-voxel in position n. Take, for example, 5 contiguous slices (i–2, i–1, i, i + 1, i + 2) 4 mm thick, each of them being divided into 3 sub-slices. Let us also assume that, for the thickness of the slices in question, the distribution function of the signal is a gaussian function with a standard deviation of σ = 1,8 mm. Numeric calculation on the basis of this gaussian function shows that the relative contribution of slice i to sub-voxel n is 0.76, and that of slice i-1 is 0.33. The weighting factors are then $\xi_{i,n}$ = 0.76/(0.76+0.33) ≈ 0.7 and $\xi_{i-1,n}$ = 0.33/(0.76+0.33) ≈ 0.3.

$$\mu_n'' = (\xi_{n,i} \cdot \mu_i' + \xi_{n,i-1} \cdot \mu_{i-1}' + \xi_{n,i+1} \cdot \mu_{i+1}') \quad (16)$$

where : μ_i', μ_{i-1}', μ_{i+1}' are the degree of membership of the original voxels in the vicinity of the sub-voxel *n* and belonging to the slices *i*, *i*–1, *i* + 1; $\xi_{n,i}$, $\xi_{n,i-1}$, $\xi_{n,i+1}$ are the weighting coefficients obtained from the signal slice profile of slices *i*, *i* + 1, *i*–1 in the sub-voxel *n* (figure 6).

Finally, using the marching cube algorithm [24], an iso-surface was determined for visualization and quantification. This surface, which delineates the vascular structure from the background, was determined using a degree of membership threshold of 0.5. The choice of this value was justified by a previous study which has shown the robustness and the low variability of the segmentation resulsts when using threshold value from 0.2 to 0.8 [15].

IV. RESULTS

Volume ratio (VR) was 1.130 ± 0.09; automatic volume is slightly larger than manual volumes (Wilcoxon test, $p < 10^{-4}$). Volume Overlap (VO) and correctly delineated volume (VC) were 0.784 ± 0.05 (min.: 0.71, max.: 0.86) and 94.7 ± 3.3 (min: 0.89, max 0.99) respectively.

Figure 7 shows a comparison between manual and automatic segmentation for a patient. Figure 8 shows a volume rendered after delineation and reconstruction.

V. DISCUSSION

Different automated organ delineation methods have been studied in radiotherapy treatment planning. Automated 2D contouring aimed at robust detection of organ boundaries in 2D slices. Bueno *et al.* [25] have presented a 2D morphologic approach based on watershed transformation for automatic rectum, bladder and seminal vesicles segmentation. A good segmentation accuracy has been reported for the tested slices (1.2 to 1.7 mm average distance to ground truth for bladder and rectum respectively), but no validation of complete 3D data sets has been done. Mazonakis *et al.* [26] have proposed a region growing technique for the segmentation of prostate, bladder and rectum on CT images but a slider was used to define three independent threshold ranges and consequently this method cannot be considered as automatic. Lee *et al.* [27] have recently presented a semi-automatic segmentation of nasopharyngeal carcinoma in MR images. Concerning

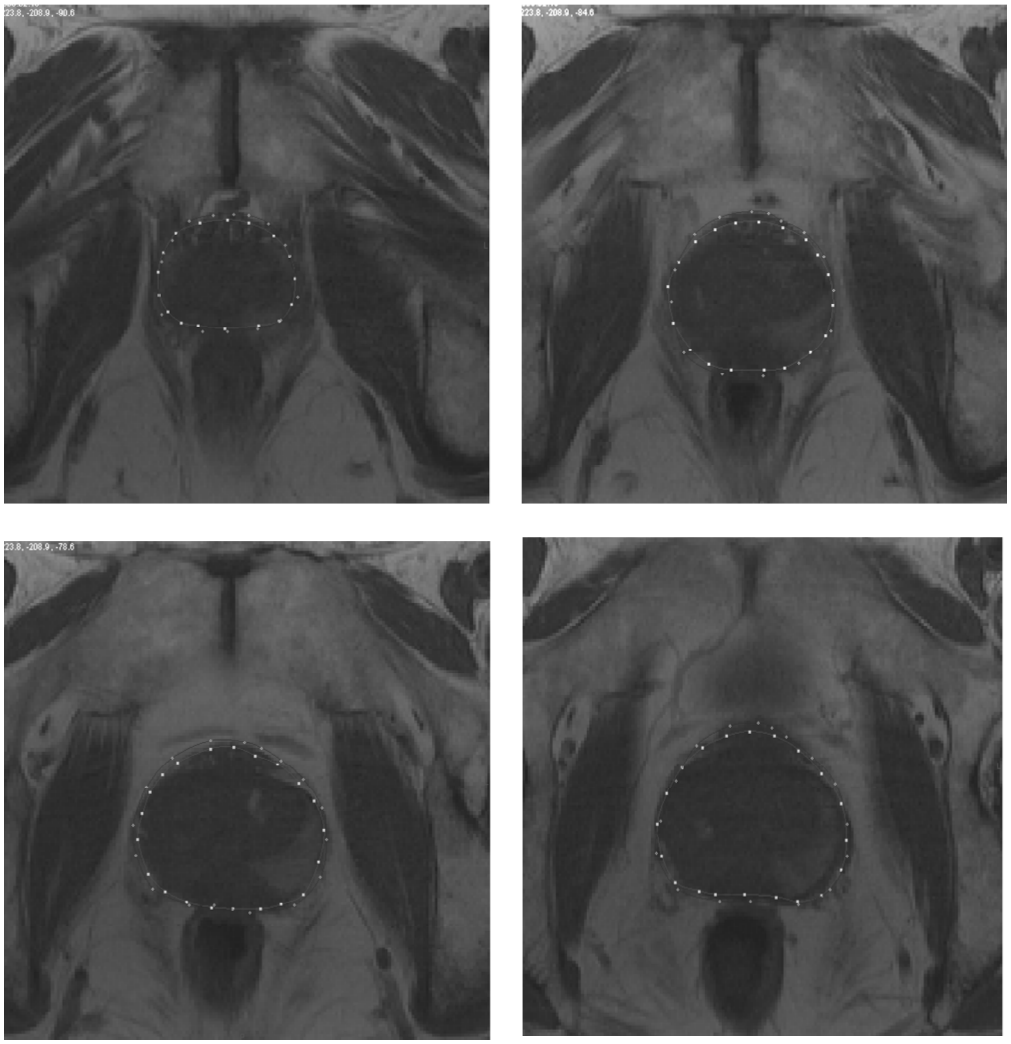

Figure 7: Comparison between automatic prostate delineation and manual delineation by an expert

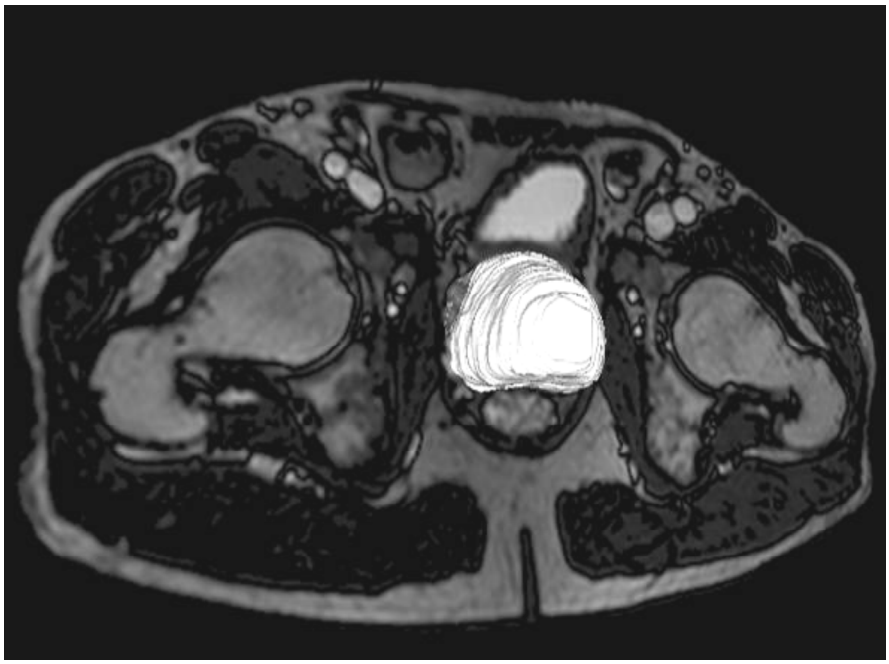

Figure 8: Final volume of the prostate

prostate automatic delineation most of the authors consider organ model based segmentation as a promising method but no detailed evaluation has been published to date. Pekar *et al*. [10] have proposed an automated model based organ at risk (rectum, bladder and femoral heads) delineation on TDM images. Reproducible and accurate results for automatic brainstem and kidney delineation have also been found with this model based method in Rao *et al.* [28] and Bondiau *et al*. [29]. Broadhurst *et al.* [30] in their method based on m-reps [7] and statistical modelling of non-parametric histograms built a prostate and rectum models from 17 images of a single patient. Although the approach is interesting, it remains far from the practice since it is evaluated on the same data having been used to build the models. In Lu *et al.* and Foskey *et al.* [11, 12] the key idea is the use of the result of a deformable image registration to match two CT exams and automatically replace manual segmentation initially laid out on the reference image. The method provides good results for intra-patient exams but suffers of weakness for inter-patients exams because of the assumption of conservation of voxels values. Freedman *et al.* [9] combined a shape-appearance model and a probability distribution of photometric variables inside the object to segment the prostate and the rectum. The authors reported major user interactions to correct the results.

Our study is one of the first to propose a truly 3D evaluation of an automated model based prostate delineation and consequently, our results are difficult to compare to others previous reports using a wide range of mainly 2D evaluation methods. Some authors have used the distances between the automatic and the manual contours (Haussdorf and radial distances). Also Pekar *et al.* [10] have compared automatic and manual rectum, bladder and femoral head contours; manual delineation was performed by a single observator. A good overall delineation accuracy (mean error 1.7 mm for bladder) was achieved but no 3D evaluation has been done. A 3D evaluation is also missed in Mazonakis *et al.* [26] where prostate, bladder and rectum volumes have been compared but on a slice-by-slice basis only. We have also to point out that a comparison based on volume index is more sensitive to small overlap differences than a comparison based on Haussdorf or radial distances. For example, two voxel cubes of 10 x 10 x 10 shifted by one voxel along the space diagonal direction results in only a 57 % volume overlap (729/1271) although the mean distance of surfaces is around one voxel. In the same way we compared radial distances and overlap volume in one patient after shifting the prostate volume by 5 voxels along the space diagonal direction in the axial plane, resulting in a maximal distance of 4 mm between automatic and manual volume: VO and VC were respectively 0.77 and 87%.

Manual segmentation is considered as the reference but cannot be considered as a perfect ground truth due to inter-observer variability. Cazzaniga *et al.* [31] have assessed the variability between 6 physicians in defining the prostate on CT for three prostate tumour cases, the percentage differences between the measured volumes and the mean values (100 x (volume – mean volume)/mean volume) were ranged from 53.6 % to 60.5 %. Fiorino *et al.* [32] and Seddon *et al.* [33] have evaluated inter-observer difference in delineating prostate on CT between 5 and 15 physicians respectively. The variation in volume was estimated at 10% (±18) and 10 % (±15) respectively.

This variability has led *Vial et al.* [15] to propose a solution for reducing this variability while improving the volume quantification from manual delineation. This method has been applied on the automatic delineated structure because the contours obtained were closed to the expert ones. Indeed, even if the variability of the automatic delineation approach is lower than the manual way and more precise according to the image segmentation, the contours obtained did not necessary provide a good volume estimation due the inherent image partial volume effect what is corrected thanks to the reconstruction step of our framework.

Note that we do not discuss about the evaluation of this fuzzy approach because it has been already validated earlier [15, 21].

V. CONCLUSION

We have developed and evaluated a new MR images anatomy automatic delineation tool based on a deformable model and a fuzzy set approach for volume quantification. We have found good accuracy but also robustness of our algorithms on a 24 prostate cancer cases evaluation study. However automatic delineation could be compared to contours made by a panel of experts to definitely confirm its robustness and reproducibility. To our knowledge, our study is one of the first 3D evaluation of an automated model based prostate delineation. Software developments are ongoing to further reduce the process time calculation allowing a daily routine use. It is probably of importance to evaluate the influence of this new automated delineation on inter-observer delineation variability and dosimetry.

Whatever segmentation technique used (manual, automatic or semi-automatic), the ultimate gold standard is, and will remain, the clinical expert's eye. The goal of the automated procedures is to relieve as much as possible the physician of time consuming tasks while assuring accuracy and reproducibility at least as high as manual method. However there is also some other parameters to take into account as the national or international regulation as well as the software conformance to the professional recommendations. Collaboration with expert committees and industrial partners that respect the standards in use could contribute to the validation and a larger spreading of these techniques.

REFERENCES

[1] Kass M. Witkin A. Terzopoulos D. Snakes: Active contour models. *Int. J. Comput.Vis.* 1(4): 321-331. 1988.

[2] Terzopoulos D. Platt J. Barr A. Fleischer K. Elastically deformable models. *Computer Graphics* 21(4): 205-214. 1987.

[3] Cootes T. F. Hill A. Taylor C. J. Haslam J. The use of Active Shape Models for locating structures in Medical Images. *Image Vision and Computing* 12(6): 355-366. 1994.

[4] Staib Lawrence H. Duncan James S. Model-based deformable surface finding for medical images. *IEEE Trans. Med. Imag* 15(5): 720-731. 1996.

[5] Shen D. Davatzikos C. An adaptive-focus deformable model using statistical and geometric information. *IEEE Trans. Pattern Anal. Machine Intell.* 22(8): 906-913. 2000.

[6] Tsai A. Yezzi A. Wells W. Tempanu C. Tucker D. Fan A. Grimson E. Willsky A. A shape based approach to curve evolution for segmentation of medical imagery. *IEEE Trans. Med. Imag* 22(2): 137-154. 2003.

[7] Pizer Stephen M. Fletcher Thomas P. Sarang Joshi Gash Graham A. Stough J. Thall A. Tracton G. Chaney Edward L. A method and software for segmentation of anatomic object ensembles by deformable m-reps. Medical Physics 32(5): 1335-1345. 2005.

[8] Cootes T. F. Taylor C. J. Statistical models of appearance for medical image analysis and computer vision. 4322 (Proc. SPIE Medical Imaging], 236-248. 2001. San Diego, CA.

[9] Freedman D. Radke Richard J. Zhang Tao Yongwon Jeong Lovelock M. Chen George T. Y. Model-based segmentation of medical imagery by matching distributions. *IEEE Trans. Med. Img.* 24(3): 281-292. 2005.

[10] Pekar V, McNutt Todd R, and Kaus Micheal. Automated model-based organ delineation for radiotherapy planning in prostatic region. *Int. J. Radiat. Oncol. Biol. Phys.* 60(3): 973-980. 2004.

[11] Lu W., Chen M. L., Olivera G. O., Ruchala K. J., Mackie T. R. Fast free-form deformable registration via calculus of variations. *Phys. Med. Biol.* 49:3067-3087. 2004.

[12] Foskey M., Davis B., Goyal L., Chang S., Chaney E., Strehl N., Tomei S., Rosenman, Joshi S. Large deformation three-dimentional image registration in image-guided radiation therapy. Phys. Med. Biol. 50: 5869-5892. 2005.

[13] Mohan R., Zhang X., Wang H., Kang Y., Wang X., Liu H., Ang K., Kuban D., and Dong L. Use of deformed intensity distributions for on-line modification of image-guided IMRT to account for interfractional anatomic changes. *Int J. Rad Oncol. Biol. Phys.* 61(4): 1258-1266. 2005

[14] Wang H., Dong l, Lii M., Lee A., De Crevoisier R., Mohan R., Cox J., Kuban D., and Cheung R. Implementation and validation of a three-dimensional deformable registration algorithm for targeted prostate cancer radiotherapy, *Int. J. Rad Oncol. Biol. Phys.* 61: 7.

[15] Vial S., Gibon D., Vasseur C., Rousseau J. Volume delineation by fusion of fuzzy sets obtained from multiplanar tomographic images. *IEEE Trans. Med. Imaging* 2001; 20: 1362-1372.25-735, 2005.

[16] Betrouni N. Vermandel M. Pasquier D. Maouche S. Rousseau J. Segmentation of abdominal ultrasound images of the prostate using a priori information and an adapted noise filter. Computerized Medical Imaging and Graphics 29(1): 43-51. 2005.

[17] Besl P. J. N. D. Mckay. A Method for Registration of 3-D Shapes. *IEEE Transactions on Pattern Analysis and Matching Intelligence* 14(2): 239-256. 1992.

[18] Helstrom C. W. Statistical Theory of Signal Detection. 1968.

[19] Deriche R. Using Canny's Criteria to Derive a Resursively Implemented Optimal Edge Detector. *International Journal of Computer Vision* 1(2): 167-187. 1987.

[20] Kirkpatrick S. Gelatt CD. Vecchi MP. Optimization by simulated Annealing. Science 220, 671-680. 1983.

[21] Vermandel M, Betrouni N., Taschner C., Vasseur C., Rousseau J. From MIP image to MRA segmentation using fuzzy set theory. Comput Med Imaging Graphics (In Press). 2007.

[22] Dubois D. Combination of information in the framework of possibility theory. New York: Abidi et al., Data fusion in robotics and machine intelligence Academic; 1992.

[23] Bourel P. Gibon D. Coste E. Daanen V. Rousseau J. Automatic quality assessment protocol for MRI equipment. *Medical Physics.* 26: 2693-2700. 1999.

[24] Bloomenthal J. An Implicit Surface Polygonizer. Graphics Gems IV. Morgan Kaufmann publ. Paul S. Heckbert ed. 1994. 324-350.

[25] Bueno G., Fisher M., Burnham K., *et al.* Automatic segmentation of clinical structures for RTP: Evaluation of a morphological approach. In: Proceedings of Medical Image Understanding and Analysis (MIUA '01). Birmingham, UK: BMVA Press: 36–73, 2001.

[26] Mazonakis M., Damilakis J., Varveris H., *et al.* Image segmentation in treatment planning for prostate cancer using the region growing technique. *Br. J. Radiol* 74: 243-248, 2001.

[27] Lee F. K., Yeung D. K., King A. D., *et al.* Segmentation of nasopharyngeal carcinoma (NPC) in MR images. *Int J. Radiat Oncol Biol. Phys.* 61: 608-620, 2005.

[28] Rao M., Stough J., Chi Y. Y., *et al.* Comparison of human and automatic segmentations of kidneys from CT images. *Int J. Radiat Oncol Biol Phys,* 61: 954-960, 2005.

[29] Bondiau P.Y., Malandain G., Chanalet S., *et al.* Atlas-based automatic segmentation of MR images : validation study on the brainstem in radiotherapy context. *Int J. Radiat Oncol Biol Phys.*, 61:289-298, 2005.

[30] Broadhurst R.E., Stough J., Pizer S.M., and Chaney E.L., Histogram Statistics of Local Model-Relative Image Regions. in International Workshop on Deep Structure, Singularities and Computer Vision (DSSCV), Lecture Notes in Computer Science Vol. 3753, of Olsen, L Florack, and A. Kuijper, eds: 71-82, (2005).

[31] Cazzaniga LF, Marinoni MA, Bossi A, *et al.* Interphysician variability in defining the planning target volume in the irradiation of prostate and seminal vesicles. Radio. Oncol., 47: 293-296, 1998.

[32] Fiorino C, Reni M, Bolognesi A, et al. Intra- and inter-observer variability in contouring prostate and seminal vesicles: implications for conformal treatment planning. Radio. Oncol., 47(3): 285-292, 1998.

[33] Seddon B, Bidmead M, Wilson J, et al. Target volume definition in conformal radiotherapy for prostate cancer: quality assurance in the MRC RT-01 trial. Radio. Oncol., 56: 73-83, 2000.